Nonuniform Cooling in Multifilament Melt Spinning of Polypropylene Fibers: Cooling Air Speed Limits and Fiber-to-Fiber Variations

ERIK ANDREASSEN,[1,*] OLE JAN MYHRE,[2] FRØYDIS OLDERVOLL,[1,†] EINAR L. HINRICHSEN,[1] KRISTIN GRØSTAD,[2,‡] and MARIANNE D. BRAATHEN[2]

[1]Sintef, P.O. Box 124 Blindern, N-0314 Oslo, Norway, and [2]Borealis AS, N-3960 Stathelle, Norway

SYNOPSIS

The cooling of the spinning stage in a commercial compact-spinning line has been studied. A rectangular fiber bundle is extruded from the spinneret and cooled by air entering from one side. The speed of the cooling air is considerably reduced through the fiber bundle. There are practical lower and upper limits for the cooling air entrance speed, corresponding to filament breakage at the leeward and windward sides, respectively. These limits are functions of the material and processing parameters. Due to the nonuniform cooling, fibers sampled at the windward side generally have higher molecular orientation, lower amorphous fraction, higher density, and higher tensile modulus and strength. For most combinations of spinning and material parameters, the structure is either bimodally oriented α-crystalline or uniaxially oriented mesomorphic at all spinneret positions. Fibers with different structure types show opposite windward/leeward side trends with regard to local order and melting behavior. The structure may be mesomorphic at the leeward side and α-crystalline at the windward side, if the average spin-line stress is close to a critical value for orientation-induced crystallization, and the air speed difference across the spinneret is large. The cooling air speed affects the spin-line stress. Hence, the fiber-to-fiber variations due to nonuniform cooling are discussed in terms of the molecular orientation in the melt and the effective time available for arranging molecules into ordered structures.

INTRODUCTION

In the compact-spinning process, the number of filaments emerging from the spinneret is typically between 5000 and 40,000. The main differences between compact (also known as short-spin) and conventional processes are summarized in refs. 1 and 2. There are two methods for cooling the fibers in the compact-spinning process: transverse, and radial flow of cooling air. In the former case, the cooling air blows perpendicular to a fiber bundle, which usually is rectangular. Hence, the fiber properties vary from the windward side to the leeward side. Also, because all the fibers are cooled asymmetrically, their structure will not be symmetrical relative to the fiber axis. This asymmetry leads to crimp. In some cases, the fiber-to-fiber variations and the crimp of fibers produced with transverse cooling are desireable, i.e., they enhance the subsequent processing of fibers, as well as the properties of end products.

Ziabicki[3] summarized some theoretical and experimental studies of the air speed and temperature fields in fiber bundles, which had been published in Polish and Russian journals in the seventies. Transverse flow of cooling air was used in these studies. The air velocity decreased and the temperature increased through the bundle. The increase/decrease was largest near the spinneret. Chen et al.[4]

* To whom correspondence should be addressed.
† Current address: Department of Chemistry, University of Oslo, P.O. Box 1033 Blindern, N-0315 Oslo, Norway.
‡ Current address: Dyno Industrier AS, Svelleveien, N-2000 Lillestrøm, Norway.

Journal of Applied Polymer Science, Vol. 58, 1619–1632 (1995)
 CCC 0021-8995/95/091619-14

compared fibers cooled by transverse flow and radial flow (inwards, perpendicular to a circular bundle). The latter cooling technique yielded fibers with symmetrical structure. Hence, the crimping behavior was eliminated. Radial cooling does not necessarily produce fibers without crimp: Paris et al.,[5] for instance, analyzed the crimp of fibers produced with this kind of cooling. Hotter et al.[6] studied a multifilament spinning line equipped with a thermal conditioning chamber, consisting of a combination of heating and cooling zones, with radial air flow. With this chamber, they claimed that the threadline temperature profile could be altered in such a way as to significantly enhance the spinning performance, as well as the fiber structure. Fourne[7] discussed transverse vs. radial flow of cooling air. Computer simulations of multifilament melt spinning of poly(ethylene terephtalate)[8-10] have provided estimates for interfilament variations that are in qualitative agreement with experimental observations. Multifilament spinning may also lead to special problems upstream of the spinneret. Koelling and Prud'homme[11] studied instabilities in multihole converging flows.

This article consists of two main sections. The first section deals with the lower and upper limits of cooling air speed, corresponding to breakage at the leeward and windward sides, respectively. The relationships between these limits and material and processing parameters are discussed. Differences between fibers from the leeward and windward sides are reported in the second section, with emphasis on structural aspects and tensile properties.

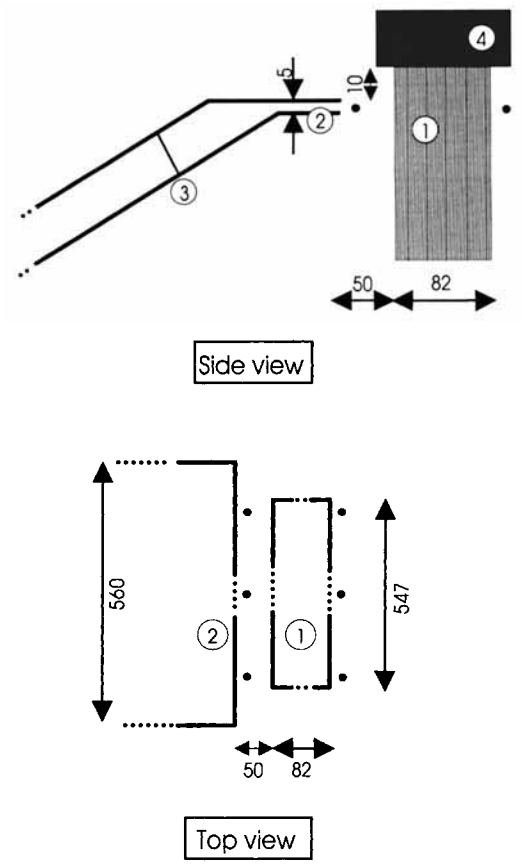

Figure 1 A schematic representation of the cooling system employed in this study. All dimensions are given in millimeters. Symbols: circled 1, fiber bundle; circled 2, cooling air slit; circled 3, wire grid; and circled 4, spinneret. The cooling air speed was measured at points marked with a solid circle.

EXPERIMENTAL

A Barmag FE1 full-scale compact-spinning line was used in this study. This line consists of three integrated stages (spinning, drawing, and annealing), but only fibers taken out directly after the spinning stage are considered in this article. Initially, there was some concern that the properties of these fibers would change considerably the first days after spinning. However, tensile testing and DSC analysis at different times after spinning (from a few minutes up to 8 weeks) revealed only minor variations. A rectangular spinneret (547 × 82 mm) with 9037 orifices with exit diameter 0.4 mm was used.

Some details of the cooling arrangement are shown in Figure 1. The cooling air speed was measured at six positions in a horizontal plane containing the cooling air slit; three at the windward side of the fiber bundle, and three at the leeward side. There were no trends among the three measurements at the same side of the bundle. Hence, only average values of the cooling air speed are considered below: v(A) at the windward side and v(B) at the leeward side. The velocity profile broadens through the fiber bundle. Hence, above and below the horizontal plane containing the cooling air slit, the differences in air speed deviate from those measured.

The temperature of the incoming cooling air was 18°C. Temperatures at the leeward side were in the range 30–40°C. The leeward side temperature depends on the extrusion rate and the extrusion temperature. The former was constant in our study. The amount of heat extracted from a fiber, in a given horizontal position, increases with increasing cooling air velocity. The temperature in the vicinity of leeward side fibers decreases with increasing cooling air speed, even though more heat is transported from

upstream fibers, because the heat is removed at a higher rate. The temperature field is also affected by radiation from the hot spinneret. However, cooling air temperatures will not be considered in the following. The reason for this is that, compared to the cooling air speeds, these temperatures do not change much from one set of experimental conditions to another, at a given spinneret position.

A reduced factorial design was employed for the variation of extrusion temperature, draw-down ratio, polydispersity index (M_w/M_n) and cooling air speed (Table I). The draw-down ratio is the ratio of take-up (spinning) speed to extrusion speed. The latter was 0.26 m/min for all the trials. The cooling air speed was varied in two levels, corresponding to filament breakage in position A and B, respectively. Trial F9 is a "midpoint" trial, for which the cooling was adjusted to be optimal. For each of the nine parameter sets in Table I, fibers were collected at position A and B (referred to as FxA and FxB, respectively, where x is the sample number in Table I). In both cases, approximately 25% of the bundle width (82 mm) was sampled (i.e., the middle half of the bundle was not sampled).

The two polypropylene (PP) homopolymers used in this study had slightly different melt flow indices (MI, ISO 1133): the one with M_w/M_n = 3 had MI = 25, and the other one had MI = 20. The grade with the narrow molecular weight distribution (MWD) was obtained by peroxide degradation. Hence, the high-molecular-weight tail was "removed."

The fibers were analyzed by tensile testing, density measurements, differential scanning calorimetry (DSC), and wide-angle x-ray scattering (WAXS). Qualitative WAXS results were obtained with a Laue camera. The molecular orientation, as well as the fractions of c- and a*-oriented crystallites,[2] were quantified by azimuthal scans. The degree of crystallinity and the order/crystallite size were quantified by 2θ scans (symmetrical reflection), using samples consisting of fibers that were finely cut (in liquid nitrogen) and randomly oriented. All 2θ values correspond to a wavelength of 0.15406 nm. WAXS data were corrected for background, polarization, absorption, and inelastic scattering.

EFFECTS OF MATERIAL AND PROCESSING PARAMETERS ON THE COOLING AIR SPEED LIMITS

An increase in the cooling air speed might influence the spinning in two ways: (1) directly, by increasing the cooling rate. In most cases this will lead to an increase in the spin-line stress. Diacik et al.,[12] for instance, in a study of single-filament high-speed spinning of PP, observed that the spin-line stress increased with increasing air speed for all draw-down ratios. (2) Indirectly, by cooling the spinneret asymmetrically. This will lead to a higher viscosity at the cold side prior to extrusion, which means less output from the spinneret and higher spin-line stress on this side (due to lower temperature and higher draw-down ratio). This effect is present in our study: the diameters of fibers from the windward side are typically 5–15% less than those of fibers from the leeward side (Table II).

In most cases, these effects affect the difference in structure development between the windward and leeward sides in the same way, and in the following, they will not be separated. In our study, the cooling

Table I Experimental Design[a] for the Variation of Spinning and Material Parameters

Sample	Extrusion Temperature [°C]	Draw-Down Ratio [−]	Polydispersity Index [−]	Breakage Position [−]	Cooling Air Speed at Position A[a] [m/s]	Cooling Air Speed at Position B[a] [m/s]
F1	280	192	5	A	8.0	1.8
F2	220	192	3	A	7.4	1.7
F3	280	38	3	A	17.0	7.1
F4	220	38	5	A	15.0	6.8
F5	280	192	3	B	5.0	0.9
F6	220	192	5	B	6.7	1.2
F7	280	38	5	B	8.0	1.8
F8	220	38	3	B	7.4	1.6
F9	250	115	4	no breakage	10.1	3.5

[a] The last two columns are not part of the reduced factorial design. The speed of the cooling air was adjusted in order to cause breakage at the windward (A) or leeward (B) side.

Table II Measurements of Linear Density

	Linear Density [dtex][a]	
Sample	A	B
F1	5.2	5.9
F2	4.7	5.4
F3	24.0	33.9
F4	24.7	27.8
F5	4.2	5.8
F6	4.6	5.1
F7	23.0	26.8
F8	23.0	26.8
F9	6.6	8.5

[a] 1 dtex ≡ 0.1 g/km.

air speed is reduced by 50–80% through the fiber bundle. Note that the difference in effective cooling, between the windward and leeward sides, is less than this because the cooling velocity profile is broader (perpendicular to the cooling air slit) at the leeward side. The reduction in cooling air speed is partly due to the broadening of the velocity profile and partly due to the presence of the fiber bundle. The difference in air speed across the bundle, as well as the air speed at the leeward side, increase as a function of the air speed at the windward side, cf. Figure 2. The relative difference, i.e., the difference divided by the speed at the windward side, decreases.

For all combinations of spinning and material parameters, there is a practical upper (v_{max}) and lower (v_{min}) limit for the incoming cooling air speed, corresponding to filament breakage at the windward and leeward sides, respectively. Spinning instabilities and breakage mechanisms[1,3,8,13–17] are not the key issues in this article, but some possible causes for breakage are mentioned in the next two paragraphs.

Breakage at the windward side, when the cooling air reaches v_{max}, could be explained by either the normal drag force[18] or the stress in the melt exceeding critical values. The fact that v_{max} increases with decreasing spin-line stress (increasing extrusion temperature and decreasing draw-down ratio) disfavor the former hypothesis, because the bowing of fibers will increase with decreasing spin-line stress.[1] The decrease in v_{max} with increasing spin-line stress is, however, consistent with the hypothesis that breakage occurs at a critical spin-line stress (i.e., cohesive melt fracture).[3] Also, at a higher draw-down ratio, the filaments are thinner and they move faster. This, again, leads to an increased cooling rate. Hence, the draw-down ratio affects the spin-line stress both directly and indirectly.

When the cooling air speed is lower than v_{min}, the extrudates break up at the leeward side. The mechanisms involved in this spinning regime are less clear.[1,3,8] Periodic or nonperiodic fluctuations in fiber diameter and spin-line stress may be responsible for the breakage.[3,15,16] Such fluctuations can be induced by fluctations in external conditions, but they can also be internal instabilities. Yoo[16] claimed that the spinning of PP is stabilized by increasing the cooling, because the critical strain, at which the elongational viscosity starts to decrease, increases with increasing cooling. (According to Yoo, the "draw resonance" phenomenon occurs when the take-up force starts to decrease with an increase in spinning speed. The take-up force is proportional to the product of elongational viscosity and elongation rate.) The stabilization by cooling may also be explained in a simpler way: consider a portion of

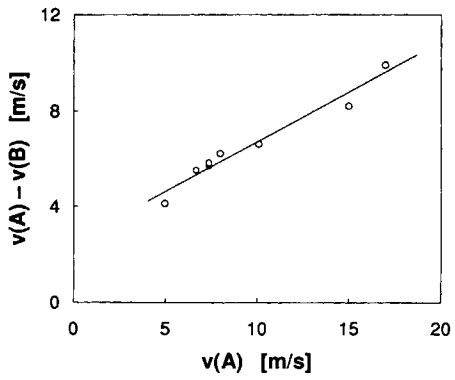

(a)

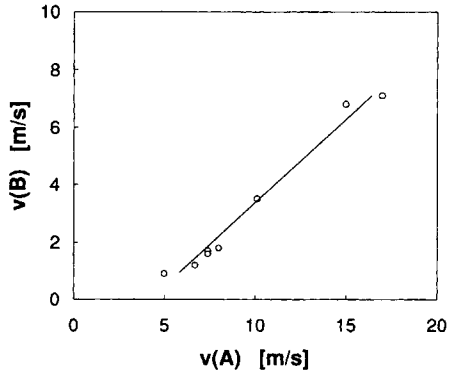

(b)

Figure 2 Cooling air speed difference across the bundle (a) and air speed at the leeward side (b) vs. air speed at the windward side. The data are taken from Table I.

the extrudate (with fluctuating diameter) some distance below the die. The thin segments of the extrudate will be drawn faster than the thick segments (as long as there is no compensating hardening with increasing elongation rate). This self-accelerating process will lead to breakage. If the cooling is enhanced, the viscosity of the extrudate will increase faster along the spin-line. Hence, the deformation will mainly occur in the hottest part of the extrudate, i.e., near the die, and not in narrow portions (local diameter minima) further down the filament.

The lower limit of cooling air speed, v_{min}, decreases with increasing draw-down ratio, but not as much as v_{max}. The decrease in v_{min} could be explained by the enhanced cooling, caused by the higher draw-down ratio, as described above. This decrease is, however, not compatible with an explanation based on draw resonance, because this phenomenon occurs above a critical draw-down ratio. v_{min} also seems to decrease with decreasing M_w/M_n. Diameter fluctations are generally smaller for a narrow MWD material,[1,16,19] because the viscosity is more homogeneous on a microscopic scale. Hence, if breakage at the leeward side is caused by diameter fluctations, more cooling is needed in order to stabilize the spinning of the broad MWD fiber, which is in accordance with our measurements.

In order to illustrate the cooling air speed "window," the data of F1A–F4A and F5B–F8B (Table I) can be represented by linear functions $v_{max}(T_e, R_d, M_w/M_n)$ and $v_{min}(T_e, R_d, M_w/M_n)$, respectively, where T_e is the extrusion temperature and R_d is the draw-down ratio. Plots of v_{max} and v_{min} are shown in Figure 3, illustrating the main trends. The effects of extrusion temperature on v_{min}, and of M_w/M_n on v_{max}, are small, and probably not significant. The "window," $v_{max} - v_{min}$, gets narrower with increasing draw-down ratio, decreasing extrusion temperature and increasing M_w/M_n.

Figure 3 shows that the cooling of the fiber bundle is a critical parameter at high draw-down ratios. When the cooling air speed "window" is narrow, the spinning is more sensitive to fluctuations in the speed of the incoming air.

A fiber producer wants to maximize his output. The diameter of the fiber is given for a certain application. Hence, for a given die, if the draw ratio must be held constant in order to have the same fiber properties, the draw-down ratio cannot be changed. In practice, the maximum possible output, i.e., extrusion rate, is usually limited by breakage occuring at the leeward side (highest temperatures). In this case, a polymer with higher M_w or M_w/M_n can be processed at a higher extrusion rate. Similarly, the throughput can be increased if the extrusion temperature is lowered. Hence, the degree of elasticity seems to govern the spinnability in this case. For high molecular weights and low extrusion temperatures, the output may be limited by the pumping power.

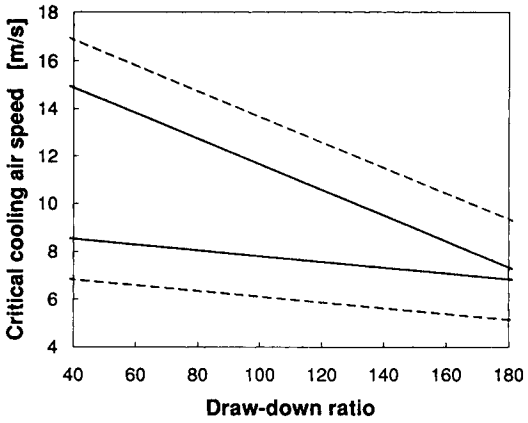

Figure 3 Schematic representation of cooling air speed "windows" for a constant extrusion speed (se main text for details). Solid lines: extrusion temperature = 220°C and M_w/M_n = 5. Dashed lines: extrusion temperature = 280°C and M_w/M_n = 3.

DIFFERENCES IN FIBER PROPERTIES BETWEEN THE LEEWARD AND WINDWARD SIDES

Nonuniform cooling will affect the fibers in two ways: (1) fibers from the windward (A) and leeward (B) sides experience different cooling histories, and will obtain different properties. Fibers sampled at position A and B will be compared in this section. Details of the sampling were given in the Experimental section. (2) The structure of the fibers may be asymmetrical relative to the fiber axis. This aspect was mentioned in the Introduction, but it will not be considered below.

Structure

The structure and morphology of the fibers is related to the spin-line stress, the high-molecular-weight tail of the MWD,[2] and the cooling rate. The spin-line stress is, of course, not independent of the two other quantities; the spin-line stress generally increases with increasing draw-down ratio, decreasing extrusion temperature, increasing cooling air velocity, and a higher fraction of high-molecular-weight chains. High spin-line stresses and/or the presence

of long chains lead to orientation-induced crystallization, and a monoclinic crystalline structure (α phase) with bimodal orientation (this structure will be referred to as type I). Alternatively, the material is quenched into a mesomorphic structure with uniaxial orientation (type II). In both cases, the orientation of structural elements increases with increasing spin-line stress.

The effects of processing and MWD parameters on the structure development in the spinning stage were discussed in an earlier article,[2] and the same trends are seen in this study: broad MWDs, high draw-down ratios, and low extrusion temperatures lead to type I structure. F1, F4, F6, and F9 all have type I structure for both windward and leeward samples (Fig. 4), while F3, F5, F7, and F8 have type II structure (Fig. 5). Windward and leeward side samples of fiber F2 have type I and II structure, respectively (Fig. 6). Hence, for F2, the spin-line stress is above a critical value for the formation of type I structure at the windward side, and below at the leeward side. This indicates that two conditions must be fulfilled in order to obtain both types of

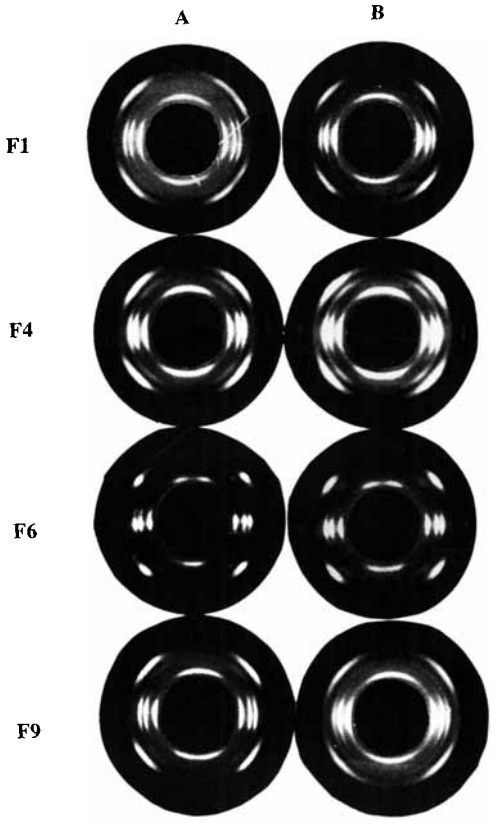

Figure 4 WAXS patterns for α-crystalline fibers (the fiber axis is vertical). Sample numbers and symbols refer to Table I.

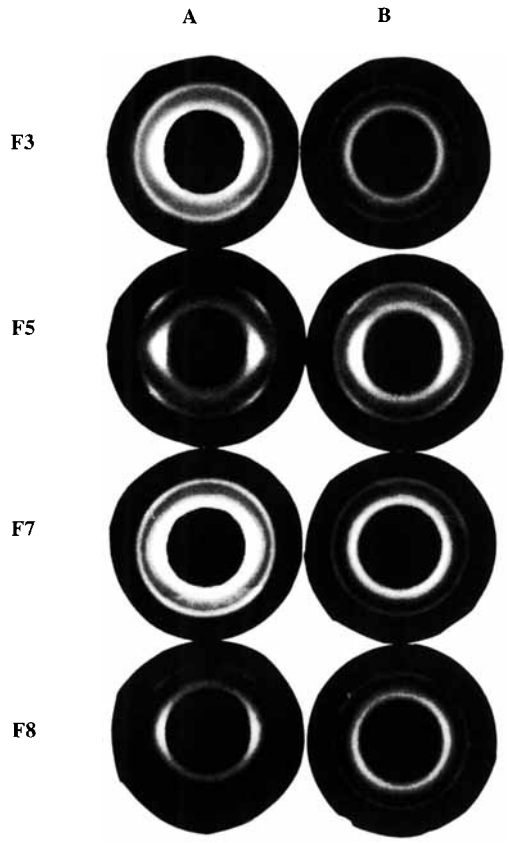

Figure 5 WAXS patterns for mesomorphic fibers (the fiber axis is vertical). Sample numbers and symbols refer to Table I.

structure: (1) the average spin-line stress (for all the fibers emerging from the spinneret) must be close to the critical value for the formation of type I structure. (2) The difference in cooling air speed between the windward and the leeward sides must be sufficiently high. As mentioned earlier, this difference increases with the speed of the incoming air.

Azimuthal and 2θ detector scans were performed in order to quantify the trends in Figures 4–6. The diffractograms were resolved into separate peaks; Gaussian for the azimuthal scans and Lorentzian

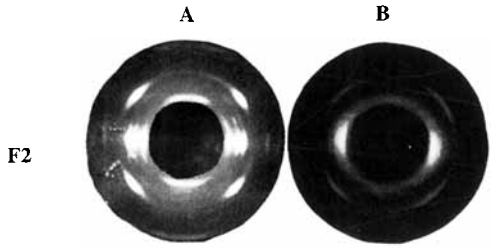

Figure 6 WAXS patterns for fiber F2.

Table III WAXS Data for α-Crystalline Fibers

	Crystalline Weight Fraction		2θ Width at Half-Maximum of 110 Peak [°]		$\bar{N}_{110}$[b]		$g_{II,110}$[c]		Fraction of Crystallites with a*-Orientation	
Sample[a]	A	B	A	B	A	B	A	B	A	B
F1	0.64	0.62	0.66	0.68	25	33	0.048	0.061	0.18	0.17
F2	0.60		0.62		25		0.043		0.11	
F4	0.73	0.69	0.49	0.53	33	29	0.038	0.039	0.24	0.26
F6	0.66	0.67	0.47	0.50	33	31	0.037	0.038	0.18	0.20

[a] F9A and F9B were not analyzed.
[b] Average number of unit cells (normal to the 110 plane) per crystallite (see text for further details).
[c] Average relative distance fluctuation between successive 110 planes (see text for further details).

for the 2θ scans. The 2θ scans of fibers with type I structure were separated into seven crystalline peaks (hkl = 110, 040, 130, 111, 041, 060, and 220) and one amorphous peak (2θ = 17.0°), while the diffractograms of type II fibers were separated into two major mesomorphic peaks (2θ = 14.8° and 21.3°), two minor peaks (corresponding roughly to reflections with hkl = 060 and 220), and one amorphous peak (same 2θ as for type I diffractograms). The center positions of the fitted peaks varied less than ±0.2° from one fiber sample to another.

The 2θ scan of sample F2B was the only one showing type I/II "mix." The type I fraction was small, and probably due to a few fibers originating from positions (within the "25%" leeward side sample) with the highest cooling air speed.

Azimuthal scans of the 110 reflection of bimodally oriented α-crystalline fibers were separated into contributions from the c- and a*-oriented populations.[2] Azimuthal scans of type II fibers were done for the (inner) mesomorphic peak with 2θ = 14.8°.

Relationships between data from azimuthal and 2θ scans (Tables III and IV) and material and spinning parameters were analyzed by regression analysis. Linear functions of these parameters account for most of the trends in the data, as examplified in Figure 7. The remainder of this section, which is divided into three subsections, will summarize and discuss these trends. As mentioned above, the spin-line stress and the MWD are the key parameters influencing the structure development. A third parameter, which is important for the degree of crystallinity and linked to the spin-line stress, is the residence time in a temperature/stress interval with

Table IV WAXS Data for Mesomorphic Fibers

	Mesomorphic Weight Fraction		2θ Width at Half-Maximum of First Mesomorphic Peak [°]		Relative Area of Second Mesomorphic Peak (A_{2rel})[a]		Azimuthal Width at Half-Maximum of First Mesomorphic Peak [°]	
Sample	A	B	A	B	A	B	A	B
F2		0.63		2.4		0.49		39
F3	0.61	0.60	2.7	2.6	0.46	0.50	58	95
F5	0.59	0.57	2.8	2.8	0.40	0.41	45	61
F7	0.63	0.60	2.6	2.6	0.53	0.50	100	103
F8	0.63	0.61	2.7	2.7	0.46	0.52	66	92

[a] The peak areas were integrated weighted with a $\sin^2\theta$ factor, as in the calculation of mesomorphic and crystalline weight fractions.[22]

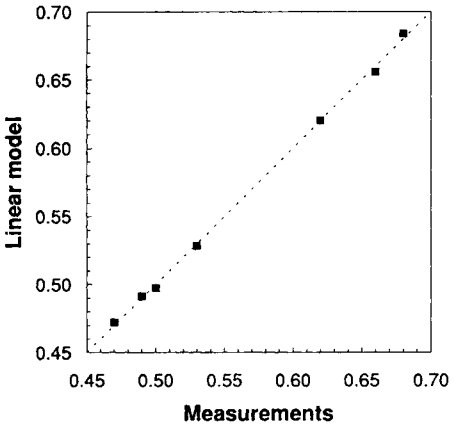

Figure 7 Predictions by a linear function, $f(M_w/M_n$, extrusion temperature, draw-down ratio, cooling air speed), vs. measurements for the 2θ width at half-maximum of the 110 peak (cf. Table III).

significant crystallization rates. (The degree of crystallinity is a time integral of the crystallization rate function.)

α-Crystalline Fibers

The degree of crystallinity of α-crystalline fibers (Table III) increases as M_w/M_n, the spin-line stress, and the residence time mentioned above increase. The spin-line stress increases, while the residence time decreases with increasing draw-down ratio (as mentioned above, the extrusion speed is the same for all the fibers in this study). Hence, the influence of draw-down ratio on the degree of crystallinity is a result of two competing effects (and, therefore, not well described by the linear models mentioned in the preceding paragraph). The F4 pair is more crystalline than the F6 pair. Hence, in this case the residence time effect probably dominates (although the cooling air speeds are higher for the F4 pair, the spin-line stresses are lower, judging from the lower orientation in Fig. 4).

Crystallinity values very close to those in Table III have been obtained in computer simulations,[20] using the Nakamura equation for crystallization kinetics[3,21] and the following empirical rate function:

$$K(T, \sigma) = (a_1 + b_1\sigma) \times \exp\left[-\frac{1}{2}\left(\frac{\log(T/(a_2 + b_2\sigma))}{a_3 + b_3\sigma}\right)^2\right], \quad (1)$$

T is the temperature and σ is the stress. $K(T,\sigma=0)$ was fitted to data for quiescent crystallization, and the coefficients b_i were adjusted to account for the orientation-induced crystallization.

For F1 and F4, the windward samples are more crystalline than the leeward samples, while the opposite effect is observed for F6. Increasing the cooling air speed leads to increased spin-line stress and a higher cooling rate. This will result in a higher value for $K(T,\sigma)$ near the spinneret, due to the higher stress. However, the increase in cooling rate will reduce $K(T,\sigma)$ further down the spin-line (Fig. 8), if the temperature effect dominates the stress effect, since $K(T,\sigma)$ goes towards zero as the temperature decreases. The final crystallinity is a result of these two competing effects (the peaks in Fig. 8 have almost the same integral; the leeward side peak has a lower maximum value, but it is somewhat broader). Preliminary simulation results suggest that the latter trend dominates for F6, because the absolute value of the temperature gradient, dT/dz, is low at the spin-line segment where $K(T,\sigma)$ is decreasing and has a higher value at the leeward side. Hence, this spin-line segment contributes more to the total accumulated crystallinity, and the highest crystallinity is obtained at the leeward side.

The 2θ width generally increases with decreasing crystallite size and increasing disorder. Methods for the separation of size and order effects[22] require at least two well-resolved orders of reflection from a given set of hkl planes. Although our data sets are marginal in this respect, Hosemann's method[22] was applied, using the two pairs available (040/060 and 110/220). Data obtained with the latter pair are shown in Table III. The distortion parameter ($g_{II,110}$) increases and the size parameter ($\bar{N}_{110}$) decreases

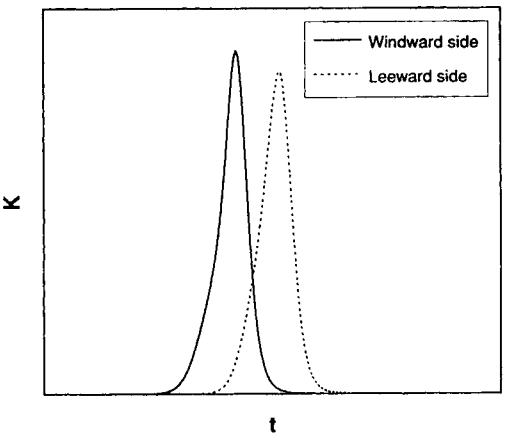

Figure 8 Schematic illustration of crystallization rate vs. time along the spin line at the windward and leeward sides.

with increasing 2θ width, with a few exceptions. The distortion parameter has the highest correlation with the 2θ width. The distinction between crystallite order and crystallite size is less clear for polymers than for low-molecular-weight substances, because the crystallite boundaries may not be well defined (in some cases it is more useful to distinguish between local order (e.g., packing of adjacent helices) and long-range order). Hence, we interpret the inverse peak width as an effective order parameter for the direction perpendicular to the corresponding hkl plane.

The 2θ widths of the 110 peaks are tabulated in Table III. Widths of other α peaks follow the same trends. The order increases with increasing spin-line stress and M_w/M_n. The main effects are those of the extrusion temperature and M_w/M_n. Fibers at the windward side experience higher spin-line stress and, hence, obtain higher order. This must be related to the mechanism of orientation-induced crystallization; high molecular orientation in the melt leads to ordered structures. Note that the F6 pair seems to have the highest (local) order, while the F4 pair has the highest degree of crystallinity. The order parameter seems to be a simpler function of material and processing parameters than the degree of crystallinity.

The last important structural parameter, which has been the topic of numerous studies, is the degree of molecular orientation. The F6 pair has the highest orientation (Fig. 4), due to the high spin-line stress. The differences between leeward and windward side samples are small, but the latter generally have somewhat higher orientation. The azimuthal scans of the 110 reflection were separated into peaks due to the c-oriented (primary) and a*-oriented (secondary) populations. The c-oriented fraction has the highest degree of orientation. This orientation is, however, a linear function of the orientation of the a*-oriented fraction, with slope equal to one. This is consistent with the autoepitaxial mechanism by which the a*-oriented crystallites are formed;[23-25] they are daughter lamellae on the lateral (010) faces of parent (c-oriented) lamellae.

The fraction of a*-oriented crystallites, which is a measure of the degree of autoepitaxy, is also calculated from the azimuthal scans (Table III). The two most important parameters in our experimental design are the draw-down ratio and M_w/M_n. The highest fraction is obtained when the draw-down ratio is low and M_w/M_n is high. One suggested prerequisite for the formation of two distinct populations is that after some time row nuclei carry so much of the tensile load that the melt between them can relax and form the secondary population (with the chains perpendicular to the fiber axis).[26] Hence, a high-molecular-weight tail and a certain spin-line stress are needed in order to obtain a large secondary population. If the spin-line stress is too high (as for the high draw-down ratio in our study), the molecules will be less able to relax and to crystallize with their chain axis perpendicular to the fiber axis.

Mesomorphic Fibers

Narrow MWDs, low draw-down ratios, and high extrusion temperatures lead to a mesomorphic structure. The fibers F3, F5, F7, and F8 all have mesomorphic structure, for both windward and leeward samples. Only one of the fibers with broad MWD is mesomorphic. This is F7, for which the values of all the other parameters contribute to a low spin-line stress. The mesomorphic weight fraction (Table IV), as calculated from 2θ scans, does not vary much from fiber to fiber. It is somewhat lower for the only pair with a high draw-down ratio (F5), and it is consistently higher for windward side samples. The cooling air speed probably affects the structure development via the spin-line stress; oriented chain segments are more easily packed into an ordered structure. The lower mesomorphic content for the high draw-down ratio must be due to the short time available for the ordering of molecules (the extrusion speed is the same for all the fibers).

As for the crystalline peaks, we interpret the inverse 2θ width of mesomorphic peaks as an effective order parameter. The widths of the mesomorphic peaks at $2\theta = 14.8°$ are quoted in Table IV. The order parameter decreases with increasing spin-line stress, although the differences between the fibers are small. The same trends are observed for the second mesomorphic peak. Note that this is opposite to what was observed for the α-crystalline fibers. The spin-line stress is related to the ratio of a rate characteristic for the process (related to deformation and/or cooling) to a characteristic molecular relaxation rate (ν_{proc}/ν_{mol}). A higher spin-line stress may favor ordering, by stretching out the chains, but the increase in ν_{proc}/ν_{mol} works against it, because the effective time available for ordering decreases. If the spin-line stress is above a critical value for orientation-induced crystallization, leading to α-crystalline fibers, the orientation effect seems to dominate the order parameter. For the mesomorphic fibers, with lower molecular orientation in the melt, the order parameter seems to be governed by the rate effect. (The air temperature is also higher at the leeward side, leading to a lower ν_{proc}/ν_{mol} value.)

Corradini et al.[27,28] have presented the most con-

vincing model for the mesomorphic structure so far. According to Corradini et al., the structure can be regarded as a disordered version of the α phase, characterized by (1) parallelism of roughly threefold helices, (2) average interchain distance around 0.60 nm, (3) close packing of a certain fraction of the chains, and (4) local correlation of the heights of adjacent helices. The close packing, referred to above, is the pairing of isotactic PP helices with the lowest energy.[29] The α phase contains arrangements of this kind, where the distance between helices is 0.52 nm (which is equal to the length of the b vector of the unit cell divided by 4).

The relative areas of the two major mesomorphic peaks are related to the packing of helices. Local packing and long range order are usually related—a closer packing of adjacent helices generally imply improved long-range order. The area of the peak with the highest 2θ (corresponding to d = 0.42 nm) will increase relative to that of the inner peak (d = 0.60 nm), with increasing degree of close packing. Hence, the relative area of the second peak (A_{2rel}) can be considered as an effective order parameter. The A_{2rel} values shown in Table IV convey roughly the same information as the inverse width of the peaks; the F7 pair being the most ordered and the F5 pair the least ordered. However, A_{2rel} is more sensitive. In accordance with the effect of spin-line stress discussed in the preceding paragraph, leeward side samples generally have higher A_{2rel} values. The F7 pair is the only exception from this trend. The higher order at the windward side for F7 may be related to the broad MWD of this fiber. Also, F7A and F7B have low (and almost equal) molecular orientation (cf. azimuthal widths in Table IV). The rate effect mentioned above may not be the limiting factor for the local ordering in this case.

As expected, the degree of orientation increases with increasing draw-down ratio, increasing cooling air speed and decreasing extrusion temperature (Fig. 5 and Table IV). Windward side samples have significantly higher orientation (except for the F7 pair). F7A has the same processing parameters as F3B, except for a slightly higher cooling air speed and a lower air temperature. The main difference is the MWD. F7A has lower orientation than F3B. Hence, the orientation of the former seems to be impeded by the high-molecular-weight fraction.

Structure vs. Critical Parameters

The fibers F1A–F4A all have critical processing parameters corresponding to breakage at the windward side. However, their structures differ with respect to type and degree of orientation. The differences are related to material and processing parameters. The same is seen for F5B–F8B. Hence, fibers with different material and processing parameters are not in the same "structural state" when the cooling air speed is close to a critical value.

In an earlier section, the breakage at the windard side was ascribed to the spin-line stress exceeding a critical value—the melt strength. Judging from the WAXS patterns in Figure 4, the F6 pair experienced a higher spin-line stress during solidification than, for example, the F4 pair. Yet, only the latter fibers break at the windward side. If the melt strength explanation is correct, this means that the F4 pair experience a higher stress in the region where the breakage occur. The distinction between the critical stresses for breakage and structure development requires further studies. The critical "thermomechanical state" in which filaments start breaking at the windward and leeward sides may depend on material and processing parameters.

Density

The density measurements are shown in Figure 9. As expected, α-crystalline fibers have higher density than mesomorphic fibers. This leads to a large density difference between F2A and F2B. For most of the fibers, the highest density is obtained at the windward side. F5 and F8 do not follow this trend, but this deviation may not be significant. [The standard deviations are below 0.0010 g/cm^3 for all the measurements, except fiber F1A (0.0027 g/cm^3),

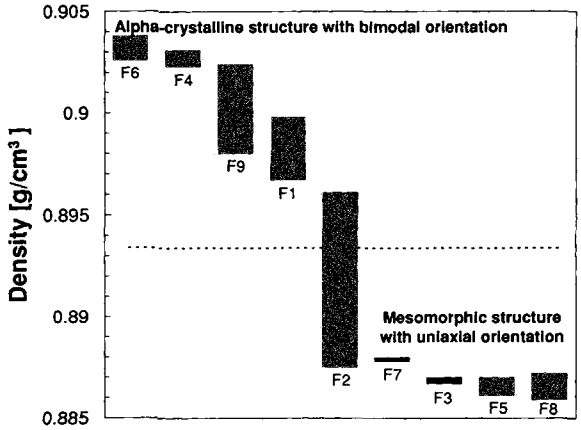

Figure 9 Density measurements. The upper and lower end of the columns refer to the windward and leeward side samples taken for each fiber. For all fibers, except number 1, 5, and 8, the highest density was measured for the windward side samples (see main text for discussion).

F8A (0.0026 g/cm^3), and F9B (0.0019 g/cm^3)]. A higher density at the leeward side for F5 and F8 may be explained by the higher order/packing, as discussed in the preceding section.

Tensile Properties

Measured tensile moduli are shown in Table V. Due to instrumental limitations, elongations above 600% could not be probed. Some of the fibers had not yet fractured at this elongation. Hence, values for the elongation and tenacity at break could not be obtained for all the fibers, and only tensile moduli and (nominal) stress–strain curves below 600% elongation will be discussed below.

Again, the fibers can be divided into two groups according to structure: type I (F1, F4, F6, and F9), and type II (F3, F5, F7, and F8). For three of the fibers in the former group, i.e., F1, F6, and F9, the tensile moduli of windward samples are typically 20% higher than those of leeward samples. Also, the windward side stress–strain curves are at a higher level (Fig. 10).

The windward and leeward side stress–strain curves of fiber F4, on the other hand, are almost the same (Fig. 11). In fact, at low and high elongations the leeward curves are somewhat higher. Furthermore, the difference between the tensile moduli of F4A and F4B is not significant. F4A and F4B experienced quite different cooling air speeds (Table I). The reason why they still have almost the same tensile properties could be that the cooling air speed at the leeward side is high, and perhaps above a critical value (F4B is the leeward sample with the highest tensile modulus). Also, since the draw-down ratio is low, the fiber is thick, and, therefore, less sensitive to changes in the cooling air speed. In any case, the deviatoric behavior of the F4 pair is probably related to its low draw-down ratio. Note that from a structural point of view (Table III), the differences be-

Table V Measurements of Tensile Moduli

	Tensile Modulus [cN/tex][a]	
Sample	A	B
F1	70	57
F2	63	45
F3	29	37
F4	90	91
F5	34	28
F6	94	77
F7	30	27
F8	31	37
F9	76	56

[a] 1 cN/tex corresponds to about 9 MPa for these fibers.

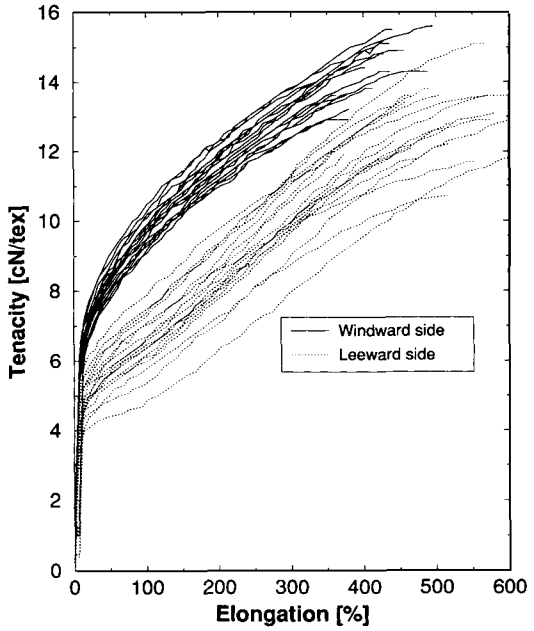

Figure 10 Stress–strain curves for F1 fibers. Twenty parallels are shown for each spinneret region.

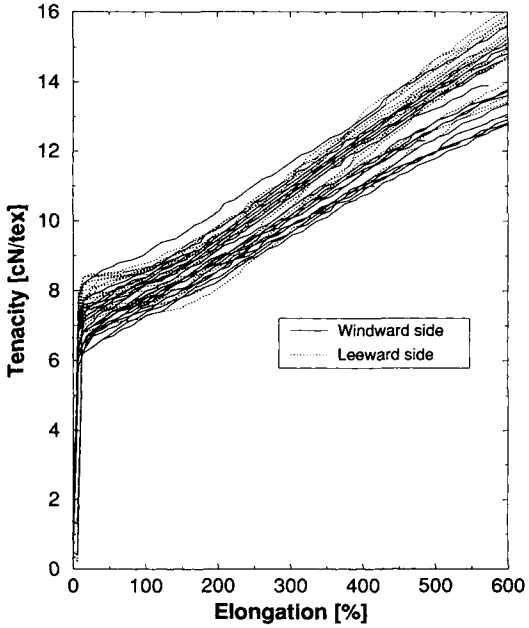

Figure 11 Stress–strain curves for F4 fibers. Twenty parallels are shown for each spinneret region.

tween F4A and F4B were similar to those observed for other α-crystalline pairs.

Windward and leeward samples with type II structure (F3, F5, F7, and F8) also differ in terms of tensile properties. The stress–strain curves of leeward samples have a plateau for elongations between 30–250%, which is absent for windward samples. Furthermore, windward samples have higher nominal stress (tenacity) at large elongations. For fiber F5, the modulus and the tenacity at all elongations are highest for the windward samples. The reason why the difference between the windward and leeward sides starts at lower elongations for this fiber could be explained by reversing the argument introduced in the former paragraph, in order to explain the small differences for fiber F4. The draw-down ratio is high, and the cooling air speed at the leeward side is very low for fiber F5. Generally, the differences between the tensile moduli of windward and leeward samples are smaller for the fibers in this group.

The tensile modulus of F2A is 40% higher than that of F2B. However, the values for tenacity at break are almost the same. This was not expected. For a given material, the tensile modulus is usually highly (positively) correlated with the tenacity at break. A similar trend was observed by Diacik et al.[12] in a study of high-speed spinning of PP: the tensile modulus increased monotonously with increasing take-up speed, but the tenacity at break started to decrease at high take-up speeds. The explanation could be that fibers spun at high spin-line stresses (high cooling air speed or take-up speed) achive high orientation, but also a high concentration of defects. The former leads to a high tensile modulus, but the latter reduces the strength. F2B samples have higher elongation at break than F2A samples. This must be due to the lower orientation and the larger diameter (Table II) of the former fibers.

Diacik et al.[12] also studied the effect of cooling air speed on the tensile properties at various take-up speeds for single-filament spinning. The spin-line stress increased with increasing cooling air speed in all cases in their study. At low take-up speeds, the tensile modulus and the tenacity at break increased, while the elongation at break decreased with increasing cooling air velocity. At high take-up speeds these trends were reversed.

There seems to be large variations in the distributions of tensile properties, such as the tenacity at break, but the number of parallels is to low for studying such trends.

DSC Melting Behavior

Principal component analysis (PCA)[30] was applied to the DSC curves. This statistical method can roughly be described as follows: consider an N-dimensional space, where the dimensions correspond to the temperatures at which the heat flow is recorded. Two DSC curves, which differ at least at one temperature, will be represented by different points in this space. The distribution of such points, for a set of DSC curves, can be characterized by an N-dimensional vector pointing in the direction with the highest variation, i.e., a line is fitted to the points. This vector is called the first principal component (PC1). Additional principal components (PCs) succesively account for as much variation as possible, within the constraint of orthogonal components. If, for instance, the points are mainly distributed in a plane, two orthogonal vectors in this plane constitute the principal components, and the "dimension" of the variation is reduced from N to 2. If the data are randomly distributed, PC1 will account for $1/N$ of the variance.

Two PCs explain 89% of the variance for the DSC curves in this study. In Figure 12, the points representing the 54 DSC curves obtained in this study (three parallels of windward and leeward side fibers for nine sets of spinning/material parameters, see Table I), are projected into the plane spanned by PC1 and PC2. PC1 separate fibers with structure types I and II. The variation between sets of spinning/material parameters and between parallels is

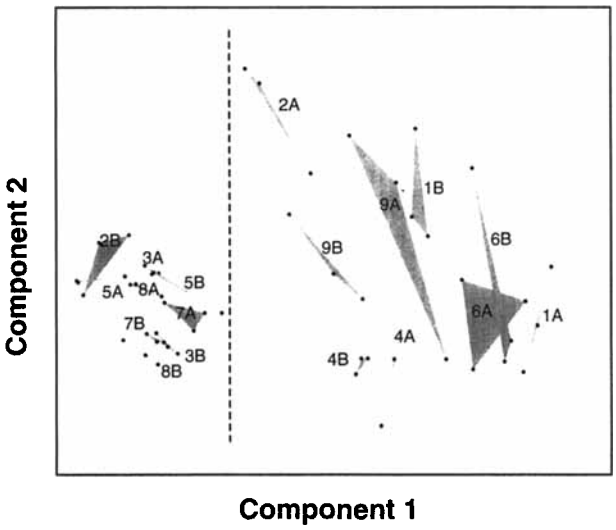

Figure 12 Score plot for the PCA of DSC curves (see main text for further details). The dashed line separates fibers with type I and type II structure.

Table VI Peak Melting Temperatures Measured by DSC

	Melting Temperature [°C]	
Sample	A	B
F1	161.3	160.6
F2	159.8	158.4
F3	159.4	160.7
F4	161.8	161.6
F5	157.7	159.7
F6	161.3	161.3
F7	160.5	160.5
F8	159.2	160.6
F9	160.8	160.9

higher for fibers with type I structure. The leeward samples of F3, F7, and F8 form a cluster. These three fibers also have similar WAXS patterns; they are mesomorphic with low orientation.

The main trends among the DSC curves are as follows: for fibers with type I structure at both positions, the windward side peaks are larger, and they are shifted towards higher temperatures (Table VI). For fiber F2, with structure type I and II at the windward and leeward sides, respectively, the trends are the same. In addition, the leeward side peak is much broader. For fibers with type II structure at both positions, the leeward side samples have the highest peak melting temperature, but their peaks are still smaller and broader.

The trends for type I fibers and F2 are similar to those observed earlier,[31] when fibers that had experienced different spin-line stresses were compared. As expected, the windward side corresponds to higher spin-line stress, and higher melting temperatures. We do not have any relevant earlier studies to compare with regarding the trends observed for fibers with type II structure. The higher melting temperatures of fibers from the leeward side is probably related to the higher value of the order parameter discussed above, as for the type I fibers. The correlation between melting temperature and perfection/size of ordered domains is well known.[31,32] The F7 pair is the only one that does not have highest order at the leeward side, and F7A and F7B have the same melting temperature.

SUMMARY AND CONCLUSIONS

The cooling air speed is considerably reduced through the fiber bundle, and the speed reduction is proportional to the entrance speed. The asymmetrical cooling also leads to higher air temperature, extrusion temperature, and extrusion rate at the leeward side of the spinneret. There is a practical lower and upper limit for the cooling air entrance speed, corresponding to filament breakage at the leeward and windward sides, respectively. These limits are affected by the draw-down ratio, the extrusion temperature, and the polydispersity of the polymer. The main effect is that the cooling air speed "window" gets narrower as the draw-down ratio increases.

Fibers sampled at different spinneret positions differ with respect to diameter, structure, tensile properties, and melting behavior. For most combinations of spinning and material parameters, the structure is either bimodally oriented α-crystalline or uniaxially oriented mesomorphic at all spinneret positions. However, the structure may be mesomorphic at the leeward side and α-crystalline at the windward side, if the average spin-line stress is close to the critical value for orientation-induced crystallization, and the air speed difference across the spinneret is large.

Samples from the windward side generally have smaller diameters, higher orientation, lower amorphous fraction, higher density, and higher tensile modulus and strength. There are some exceptions to these trends, because the two main effects of increasing the cooling air speed (increased molecular orientation and decreased effective time for structure development) in some cases work against each other.

When α-crystalline fibers are obtained at all spinneret positions, windward samples have more perfect/larger crystalline domains and higher peak melting temperatures. When the fibers are mesomorphic, however, opposite trends are observed for these two properties. This difference between α-crystalline and mesomorphic fibers may be explained by the orientation of molecules during solidification.

The magnitude of the windward/leeward side variations is related to the type of structure (α-crystalline or mesomorphic). The largest fiber-to-fiber variations are observed when different structure types are obtained at the windward and leeward sides.

The variations in structure, tensile properties, and melting behavior can be explained in terms of the molecular orientation in the melt and the effective time available for arranging molecules into ordered structures.

Nonuniform cooling may contribute significantly to the variation among fibers produced in a compact-

spinning line, although only fibers taken out directly after the spinning stage were considered in this article. Further work is needed in order to relate the spinning stage variation to that of the entire production line.

This article is based on results from the 'Expomat Fiber Project,' supported by Borealis and the Research Council of Norway.

REFERENCES

1. M. Ahmed, *Polypropylene Fibers—Science and Technology,* Elsevier, Amsterdam, 1982.
2. E. Andreassen, O. J. Myhre, E. L. Hinrichsen, and K. Grøstad, *J. Appl. Polym. Sci.,* **52,** 1505 (1994).
3. A. Ziabicki, *Fundamentals of Fibre Formation,* Wiley, London, 1976.
4. G.-Y. Chen, J. A. Cuculo, and P. A. Tucker, *J. Appl. Polym. Sci.,* **44,** 447 (1992).
5. A. Paris, J.-M. Haudin, and P. Navard, *Seventh Annual Meeting of the Polymer Processing Society,* Hamilton, Canada, 1991.
6. J. F. Hotter, J. A. Cuculo, and P. A. Tucker, *J. Appl. Polym. Sci.,* **43,** 1511 (1991).
7. F. Fourne, *Int. Fiber J.,* **3,** 30 (1988).
8. T. Matsuo, H. Yasuda, and H. Sugiyama, *Prepr. Mezhdunar. Simp. Khim. Voloknam,* **2,** 206 (1977).
9. A. Dutta, *Polym. Eng. Sci.,* **27,** 1050 (1987).
10. H. Ishihara, S. Hayashi, and H. Ikeuchi, *Int. Polym. Proc.,* **4,** 91 (1989)
11. K. W. Koelling and R. K. Prud'homme, *Rheol. Acta,* **30,** 511 (1991).
12. I. Diacik, Jr., I. Diacik, and M. Jambrich, *Acta Polym.,* **41,** 500 (1990).
13. S. Kase, *J. Appl. Polym. Sci.,* **18,** 3279 (1974).
14. C. D. Han and Y. W. Kim, *J. Appl. Polym. Sci.,* **20,** 1555 (1976).
15. M. M. Denn, *Annu. Rev. Fluid Mech.,* **12,** 365 (1980).
16. H. J. Yoo, *Polym. Eng. Sci.,* **27,** 192 (1987).
17. A. Ghijsels and J. De Clippeleir, *Int. Polym. Proc.,* **9,** 252 (1994).
18. Y. D. Ju and R. L. Shambaugh, *Polym. Eng. Sci.,* **34,** 958 (1994).
19. Q. Fan, D. Xu, D. Zhao, and R. Qian, *J. Polym. Eng.,* **5,** 95 (1985).
20. E. Andreassen, E. L. Hinrichsen, U. E. Gundersen, F. Oldervoll, and H. P. Langtangen, to appear.
21. K. Nakamura, K. Katayama, and T. Amano, *J. Appl. Polym. Sci.,* **17,** 1031 (1973).
22. L. E. Alexander, *X-Ray Diffraction Methods in Polymer Science,* R. E. Krieger Publishing Company, Malabar, FL, 1985.
23. B. Lotz and J. C. Wittmann, *J. Polym. Sci., Polym. Phys. Ed.,* **24,** 1541 (1986).
24. W. Stocker, S. N. Magonov, H.-J. Cantow, J. C. Wittmann, and B. Lotz, *Macromolecules,* **26,** 5915 (1993).
25. W. Stocker, S. Graff, J. Lang, J. C. Wittmann, and B. Lotz, *Macromolecules,* **27,** 6677 (1994).
26. A. Peterlin, in *Flow-Induced Crystallization in Polymer Systems,* R. L. Miller, Ed., Gordon and Breach, New York, 1977.
27. P. Corradini, V. Petraccone, C. De Rosa, and G. Guerra, *Macromolecules,* **19,** 2699 (1986).
28. P. Corradini, C. De Rosa, G. Guerra, and V. Petraccone, *Polym. Commun.,* **30,** 281 (1989).
29. P. Corradini, V. Petraccone, and B. Pirozzi, *Eur. Polym. J.,* **19,** 299 (1983).
30. P. Geladi and B. R. Kowalski, *Anal. Chim. Acta,* **185,** 1 (1986).
31. E. Andreassen, K. Grøstad, O. J. Myhre, M. D. Braathen, E. L. Hinrichsen, A. M. V. Syre, and T. B. Løvgren, *J. Appl. Polym. Sci.,* **57,** 1075 (1995).
32. B. Wunderlich, *Macromolecular Physics, Vol. 3. Crystal Melting,* Academic Press, New York, 1980.

Received March 28, 1995
Accepted June 25, 1995